ELSEVIER

Contents lists available at ScienceDirect

Biomaterials

journal homepage: www.elsevier.com/locate/biomaterials





T cell-responsive macroporous hydrogels for *in situ* T cell expansion and enhanced antitumor efficacy

Rimsha Bhatta^a, Joonsu Han^a, Yusheng Liu^a, Yang Bo^a, Hua Wang^{a,b,c,d,e,f,g,*}

- ^a Department of Materials Science and Engineering, University of Illinois at Urbana-Champaign, Urbana, IL, 61801, USA
- ^b Cancer Center at Illinois (CCIL), Urbana, IL, 61801, USA
- ^c Department of Bioengineering, University of Illinois at Urbana-Champaign, Urbana, IL, 61801, USA
- ^d Carle College of Medicine, University of Illinois at Urbana-Champaign, Urbana, IL, 61801, USA
- e Beckman Institute for Advanced Science and Technology, University of Illinois at Urbana-Champaign, Urbana, IL, 61801, USA
- ^f Materials Research Laboratory, University of Illinois at Urbana-Champaign, Urbana, IL, 61801, USA
- g Institute for Genomic Biology, University of Illinois at Urbana-Champaign, Urbana, IL, 61801, USA

ARTICLE INFO

Keywords: T cell therapy T cell expansion Hydrogel Immunotherapy Cell-responsive

ABSTRACT

Adoptive T cell therapy has demonstrated great promise for treating cancer and other diseases. While extensive effort has been made to improve ex vivo expansion of T cells, strategies for maintaining the proliferation and function of T cells post adoptive transfer are still lacking. Here we report an injectable T cell-responsive macroporous hydrogel that enables in situ activation and expansion of T cells. The macroporous gel is composed of a polymeric network with dispersed macropores (\sim 150 μ m) that are large enough to home T cells. In the presence of T cells that can gradually disrupt the gel network surrounding the macropores, activation cues can be gradually released for in situ activation and expansion of T cells. This T cell-responsive macroporous gel enables expansion of effector T cells in vivo, is stable over weeks upon subcutaneous injection, and results in enhanced CD8 $^+$ T cell response and antitumor efficacy. We further show that the T cell-responsive macroporous gel could comparable antitumor efficacy to conventional T cell therapy with a much lower cell dose. This injectable, T cell-responsive macroporous gel provides a platform for in vivo expansion of engineered T cells in a controlled manner, for timely and effective treatment of diseases.

1. Introduction

T cell therapy, especially chimeric antigen receptor (CAR) T cell therapy, has demonstrated great promise for cancer treatment [1,2]. In this approach, T cells are often isolated from the patient's blood, genetically modified to express CARs that can recognize a certain marker on the surface of tumor cells, expanded *ex vivo*, and infused back to the patient [3,4]. The whole process could take weeks to generate sufficient functional T cells for adoptive transfer [5–9]. Extensive effort has been made to shorten the *ex vivo* expansion process [10]. For example, artificial antigen presenting cell (aAPC) systems bearing T cell activation cues (e.g., anti-CD3 and anti-CD28) were developed to mimic natural APCs and expand T cells *ex vivo*. [11,12] Among them, dynabeads, micron-sized particles bounded with anti-CD3/CD28, have been successfully used for polyclonal expansion of CAR T cells in clinic [13]. Various biomaterial scaffolds presenting T cell activation cues, including

mesoporous silica rod scaffolds, have also been reported [11,14,15]. While these material systems enabled rapid *ex vivo* expansion of T cells, the overall T cell manufacturing process is still lengthy and costly [16], posing a hurdle for timely treatment of cancer and other diseases in clinic. The death and dysfunction of T cells during and after re-infusion could also undermine the therapeutic potential of T cell therapy [17]. These issues have motivated the development of new strategies that enable the expansion and modulation of T cells *in vivo*.

Several material systems have been developed to activate and expand T cells *in situ*. [18] In one approach, scaffolds with surface coating of T cell activation cues were implanted together with the engineered T cells at or near the tumor site, with the goal of expanding and releasing functional T cells *in situ*. [19–22] While this approach demonstrated some success for local therapy, the rapid release of T cells from the scaffold granted a limited time window for T cell expansion, often necessitating the implantation of a high initial number of T cells.

^{*} Corresponding author. Department of Materials Science and Engineering, University of Illinois at Urbana-Champaign, Urbana, IL, 61801, USA. E-mail address: huawang3@illinois.edu (H. Wang).

Another approach involved the injection of microbeads or nanoparticles bounded with T cell activation cues before or after adoptive transfer of T cells, which could traffic systemically to find and expand T cells *in vivo*. [23–26] However, the targeting efficiency for adoptively transferred T cells was rather low, and non-specific expansion of endogenous T cells in healthy tissues could pose a safety concern. Ideally, T cell activation cues should exhibit minimal background release from the material scaffold but are accessible to T cells within the materials for timely and specific expansion of T cells.

We reason that macroporous biomaterials could be a promising platform to manipulate T cells in vivo, by providing macroporous space for retaining T cells and nanoporous material matrix for storing T cell activation cues [21,27,28]. Further, in order to control the accessibility of activation cues to T cells, we aim to design a material matrix that can be disrupted by T cells and thus gradually release the trapped activation cues to T cells in the macropores. Here we report an injectable, macroporous hydrogel that enables the controlled release of microparticles from the nanoporous gel network in a T cell-responsive manner, for subsequent activation and expansion of T cells in situ (Fig. 1a). The bulk-phase gel network is composed of azido-functionalized alginate crosslinked by dibenzocyclooctyne (DBCO)-functionalized 8-arm polyethylene glycol (PEG) via disulfide linkages [29,30], while the macropores with an average diameter of $\sim 150~\mu m$ can be introduced via a cryogenation process (Fig. 1b) [31-33]. Microparticles bounded with T cell activation cues (anti-CD3 and anti-CD28) can be encapsulated in the nanoporous polymeric network, with minimal background release under physiological conditions. However, in the presence of T cells with abundant cell-surface thiol groups that can gradually disrupt the disulfide linkages [34-37], microparticles bearing T cell-activation cues can be released into the macropores to facilitate the activation and proliferation of T cells (Fig. 1a). This injectable T cell-responsive macroporous hydrogel also enables the expansion of functional T cells in vivo, for improved cytotoxic T lymphocyte (CTL) response and antitumor efficacy.

2. Results

R. Bhatta et al.

2.1. Synthesis and characterization of macroporous Alg-S-S-PEG gels

Prior to the fabrication of macroporous gels, we first synthesized DBCO-functionalized PEG and azido-functionalized alginate (Alg-N₃), respectively (Fig. 1b). DBCO-functionalized PEG was synthesized by conjugating DBCO-S-S-NHS or DBCO-NHS with 8-arm PEG-NH2, and characterized by ¹H NMR and FTIR spectrometry (Fig. S1). Alg-N₃ was synthesized via the conjugation between 11-azido-3,6,9-trioxaundecan-1-amine and sodium alginate (Fig. S2a-b). The peak at 2106 cm⁻¹ in the FTIR spectrum confirmed the successful modification of alginate with azido groups (Fig. S2b). To fabricate macroporous hydrogels, Alg-N₃ was rapidly mixed with DBCO-S-S-PEG and placed under -20 °C for over 6 h to allow for thorough click reaction, forming a crosslinked gel network with dispersed ice crystals. By bringing the gels back to ambient temperature, the ice crystals melted to form macropores within the gel network, as shown under the optical microscope (Fig. 1c) and scanning electron microscope (Fig. 1d) for both Alg-S-S-PEG and Alg-PEG gels. The resultant Alg-S-S-PEG and Alg-PEG gels are highly porous, with an average porosity of \sim 55% and pore diameter of \sim 165 μm (Fig. 1e-f, Fig. S3a). The structure and pore size of gels are dependent on the concentration and mixing time of Alg-N3 and DBCO-S-S-PEG. At high concentrations, the gel network was rapidly formed during the mixing step prior to the formation of ice crystals, resulting in the formation of gels with much smaller pores (Fig. S3b). At very low concentrations, the gel network failed to form due to the low density of covalent crosslinks (Fig. S3b). Keeping the concentration of Alg-N3 and DBCO-S-S-PEG constant, the pore size of resulting macroporous gels can be further tuned by controlling the mixing time of Alg-N3 and DBCO-S-S-PEG. By prolonging the mixing time from 25 s to 37 s, the average pore size of gels decreased from \sim 190 µm to 50 µm (Fig. 1g–h, Fig. S3c). The Alg-S-S-PEG gel has a storage modulus (G') of \sim 3600 Pa and a loss modulus (G") of \sim 200 Pa, similar to the Alg-PEG gel with a G' of \sim 3400 Pa and G" of \sim 150 Pa (Fig. 1i).

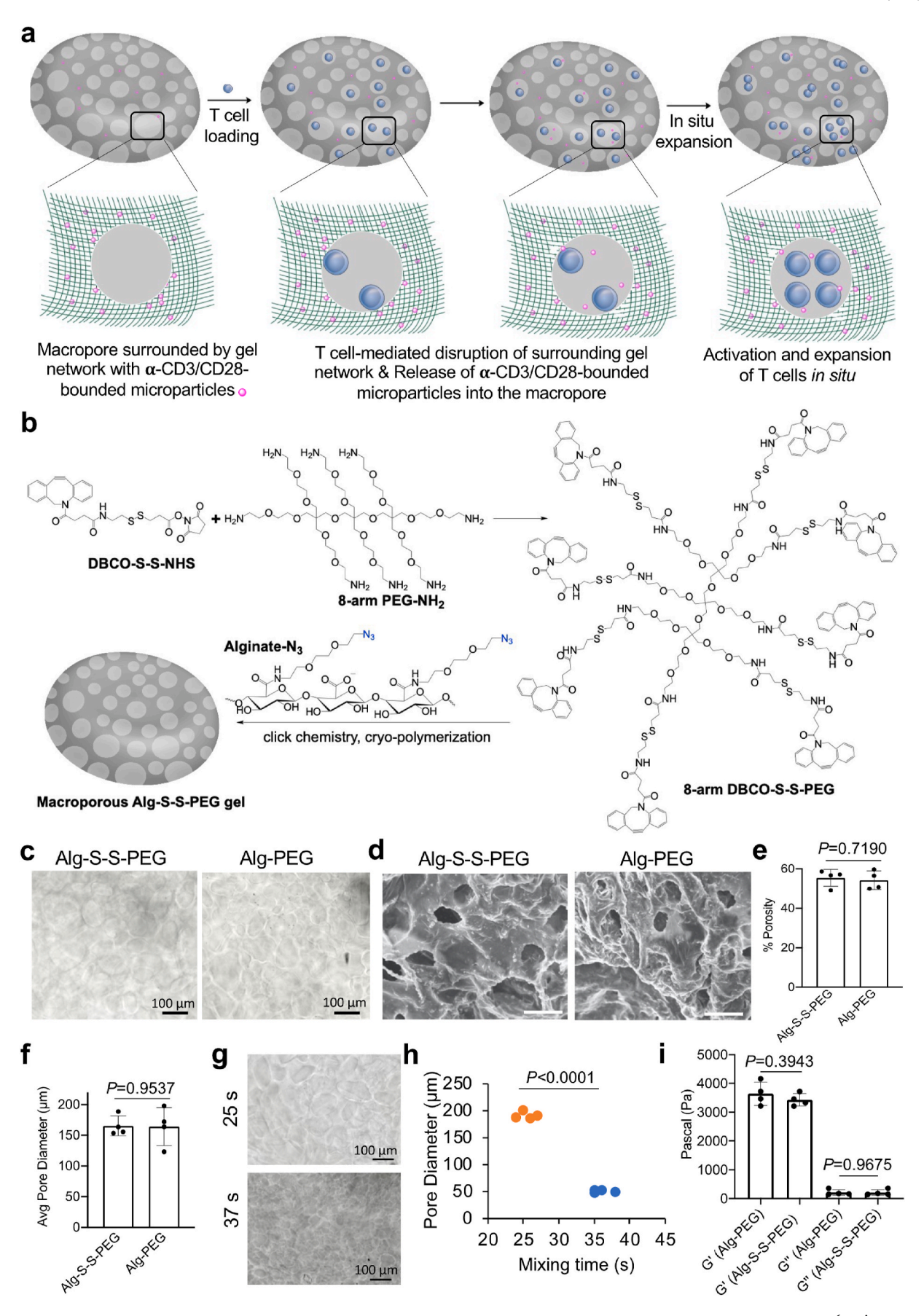
2.2. Reductive responsiveness of Alg-S-S-PEG gels

We then studied the reductive-responsive degradation of Alg-S-S-PEG gels in the presence of dithiothreitol (DTT) that can cleave the disulfide bond. After being treated with 10 μM DTT for 24 h, Alg-S-S-PEG gels remained intact, with minimal changes in morphology and macropore size (Fig. 2a and b). However, in the presence of 100 μM DTT for 24 h, Alg-S-S-PEG gels exhibited a significant decrease in storage modulus (G'), despite the maintained morphology and macroporous structure (Fig. 2a-c). In the presence of 500 µM DTT for 24 h, Alg-S-S-PEG gels were largely degraded (Fig. 2a and b). To study whether Alg-S-S-PEG gels enabled the release of microparticles in a reductiveresponsive manner, fluoroparticles (3.5 μm in diameter, $\lambda_{ex}/\lambda_{em} =$ 570/595 nm) with a similar size and structure to the commercial T cellactivating dynabeads were loaded into the gel network. Alg-N3 and fluoroparticles were co-dissolved, mixed with DBCO-S-S-PEG, and transferred to −20 °C to form the macroporous gels with well-dispersed fluoroparticles (Fig. S4a). In the presence of 500 µM DTT, Alg-S-S-PEG gels showed significant release of encapsulated fluoroparticles in 30 min, compared to the negligible release of particles from Alg-PEG gels without disulfide linkages over 24 h (Fig. 2d and e). The burst release of fluoroparticles from Alg-S-S-PEG gels in the presence of 500 µM DTT (Fig. 2e) was consistent with the degradation status of gels (Fig. 2a-c). At a lower DTT concentration (100 µM), the release of fluoroparticles from gels became slower (Fig. 2f). At 10 µM DTT, the release of fluoroparticles was even more controlled (Fig. 2g), and gels remained intact after 72 h (Fig. S4b). At all tested DTT concentrations, Alg-S-S-PEG gels showed faster release of encapsulated fluoroparticles in comparison with Alg-PEG gels (Fig. 2e-g), demonstrating the reductiveresponsiveness of macroporous Alg-S-S-PEG gels.

2.3. T cell responsiveness of Alg-S-S-PEG gels

After confirming its reductive-responsiveness, we next studied whether the Alg-S-S-PEG gel can be degraded and further enable controlled release of encapsulated microparticles in a T cell-responsive manner. While T cells entering the macroporous gel mainly stay in the macropores, we hypothesize that they can cleave off the disulfide linkages near the macropores to gradually disrupt the gel network. We first analyzed the mechanical properties of gels before and after T cell loading. T cells of different numbers could be easily loaded into the macropores of Alg-S-S-PEG or Alg-PEG gels (Fig. 3a, Fig. S5a). After loaded with T cells and incubated at 37 $^{\circ}\text{C}$ for 24 h, the storage modulus of Alg-S-S-PEG gels decreased with the initial loading density of T cells (Fig. 3b), indicating the disruption of gel network by T cells. Compared to gels (~6 mm in diameter and ~2 mm in height) loaded with 15 k T cells, gels with 150 k T cells showed a 49.6% reduction in the storage modulus after 24-h incubation (Fig. 3b). The loss modulus (G") of Alg-S-S-PEG gels also exhibited a decrease with a higher T cell loading density (Fig. 3c), but remained much lower than G' values. In contrast, Alg-PEG gels showed a negligible change in storage moduli in the presence of T cells for 24 h (Fig. S5b-c). By extending the incubation time to 48 h, G' and G" of Alg-S-S-PEG gels were further reduced in a T cell densitydependent manner (Fig. 3d, Fig. S5d).

After demonstrating that T cells can mediate the disruption of Alg-S-S-PEG gel network, we next studied whether T cells can induce the controlled release of microparticles from gels. To demonstrate, mouse $CD8^+$ T cells isolated from C57BL/6 mice were seeded into the fluoroparticle-loaded macroporous gels and incubated in a thiol-free medium at 37 °C, with the release of fluoroparticles monitored. Compared to Alg-PEG gels, fluoroparticles loaded in Alg-S-S-PEG gels



(caption on next page)

Fig. 1. Synthesis and characterization of T cell-responsive macroporous hydrogels. (a) Schematic illustration of injectable T cell-responsive macroporous hydrogels that enable controlled release of α -CD3/CD28-bounded microparticles and *in situ* expansion of T cells in a T cell-responsive manner. (b) Synthetic route and chemical structure of T cell-responsive, macroporous Alg-S-S-PEG gels. (c) Microscopic image of Alg-S-S-PEG gels and Alg-PEG gels. (d) SEM image of Alg-S-S-PEG gels and Alg-PEG gels. Scale bar: 100 μ m. (e) Porosity of macroporous Alg-S-S-PEG and Alg-PEG gels. (f) Average pore size of macroporous Alg-S-S-PEG and Alg-PEG gels. (g) Microscopic images of Alg-S-S-PEG gels fabricated via fast (25 s) versus slow mixing (37 s). (h) Average pore size of macroporous Alg-S-S-PEG gels fabricated via fast versus slow mixing. (i) Storage (G') and loss (G'') moduli of macroporous Alg-S-S-PEG and Alg-PEG gels. All the numerical data are presented as mean \pm SD (0.01 < *P \le 0.05; **P \le 0.01; ***P \le 0.001).

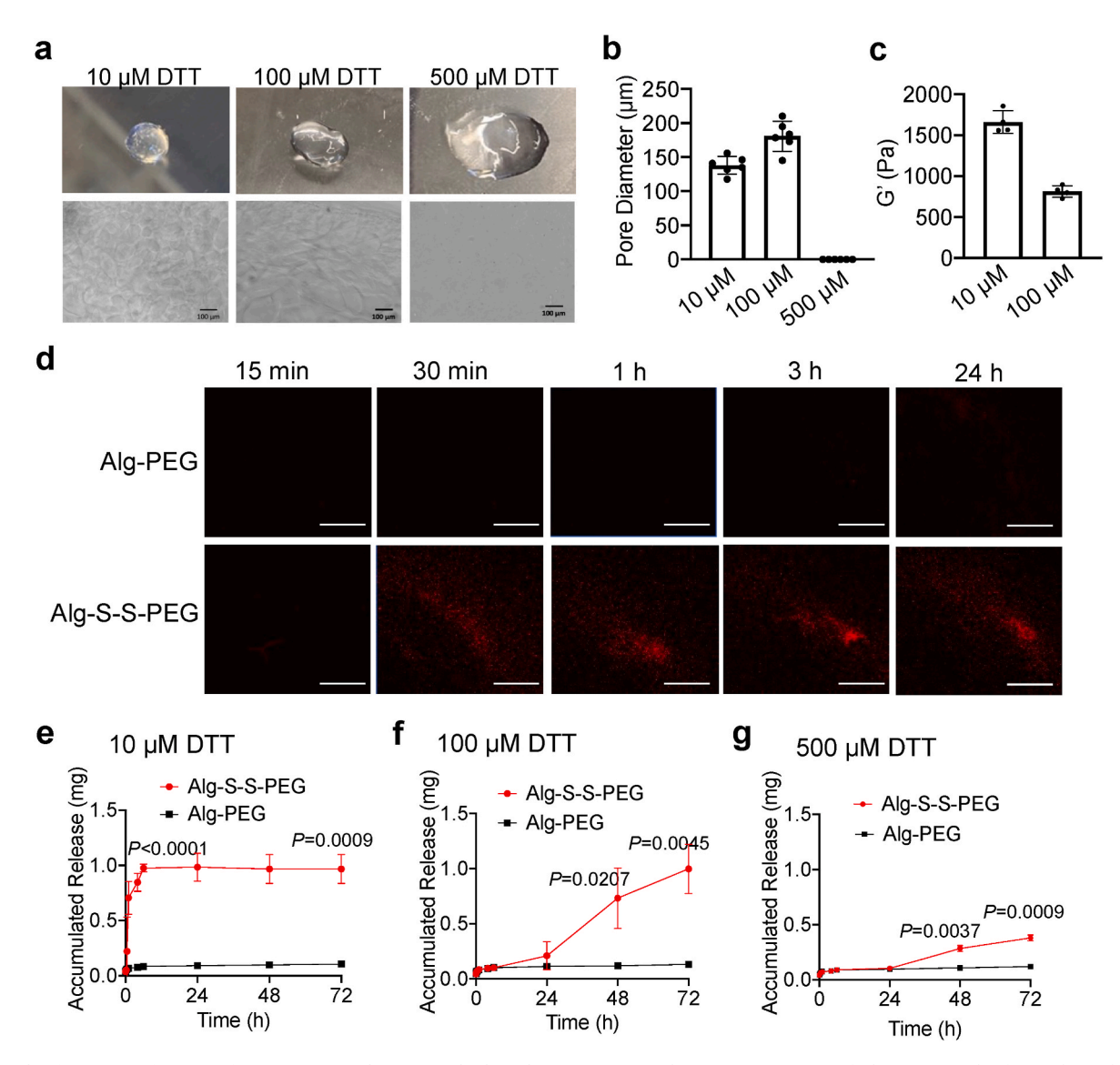


Fig. 2. Reductive responsiveness of macroporous Alg-S-S-PEG hydrogels. (a) Pictures and microscopic images of Alg-S-S-PEG gels after 24-h incubation with DTT of varied concentrations. (b) Pore diameter of Alg-S-S-PEG gels after 24-h incubation with DTT of varied concentrations. (c) Storage modulus of Alg-S-S-PEG gels after 24-h incubation with DTT of varied concentrations. (d) Fluorescence imaging of fluoroparticles released from Alg-PEG or Alg-S-S-PEG gels over time in the presence of 500 μ M DTT. Scale bar: 100 μ m. Also shown are the percentages of released fluoroparticles from macroporous Alg-S-S-PEG or Alg-PEG gels in the presence of 500 μ M (e), 100 μ M (f), and 10 μ M (g), respectively. All the numerical data are presented as mean \pm SD (0.01 < * $P \le 0.05$; ** $P \le 0.01$; *** $P \le 0.01$.

showed a significantly higher release rate at different tested T cell densities (50 k, 93 k, or 300 k per gel) (Fig. 3e–g), demonstrating T cell-mediated disruption of gel network and release of encapsulated microparticles. Considering the size of gels (\sim 6 mm in diameter and \sim 2 mm in height), 50,000 cells per gel corresponds to 885 cells per mm³ which is a very low cell density, indicating the effective disruption of gel network by T cells. The release rate of fluoroparticles remained similar when the cell density increased from 50,000 to 93,000 cells per gel and further to 300,000 cells per gel (Fig. 3e–g, Fig. S6a). We further compared the release kinetics of fluoroparticles from Alg-S-S-PEG gels with a T cell loading density of 30 k, 70 k, and 110 k per gel, respectively, which

again showed a similar release kinetics of fluoroparticles (Fig. S6b). It is noteworthy that 30 k T cells per Alg-S-S-PEG gel were sufficient to trigger the release of microparticles encapsulated in the gel network while maintaining the shape, overall structure, and storage modulus of gels, which holds great promise for long-term *in situ* expansion of T cells.

To test the relative specificity of Alg-S-S-PEG gels towards T cells, we seeded bone marrow-derived dendritic cells (DCs) in fluoroparticle-loaded Alg-S-S-PEG or Alg-PEG gels, and incubated the gels at 37 °C. Over 96 h, a minimal amount of fluoroparticles were released from Alg-S-S-PEG gels, with negligible differences between Alg-S-S-PEG gels and Alg-PEG gels (Fig. 3h). The increase in the DC loading densities, from 50

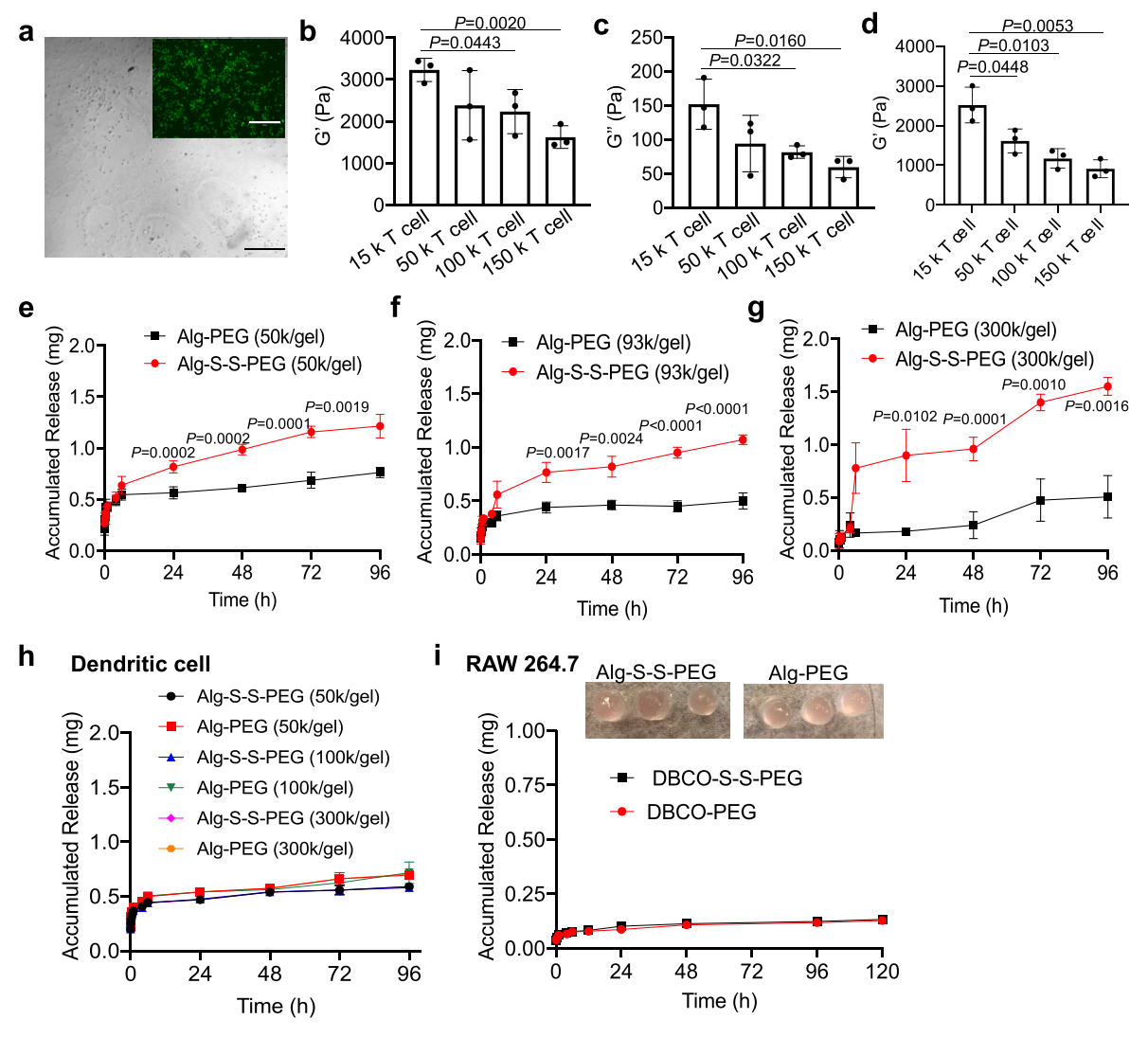


Fig. 3. T cell responsiveness of macroporous Alg-S-S-PEG hydrogels. (a) Representative microscopic and fluorescence images of Alg-S-S-PEG gels loaded with CFSE-stained T cells (100 k cells per gel). Scale bar: 200 μ m. (b) Storage modulus of Alg-S-S-PEG gels after loading with T cells of varied density for 24 h. (c) Loss modulus of Alg-S-S-PEG gels after loading with T cells of varied density for 24 h. (d) Storage modulus of Alg-S-S-PEG gels after loading with T cells of varied density for 48 h. (e–g) Alg-S-S-PEG or Alg-PEG gels encapsulating fluoroparticles were loaded with T cells of different densities and incubated at 37 °C. Shown are the release profiles of fluoroparticles from Alg-S-S-PEG or Alg-PEG gels at a cell density of (e) 50 k, (f) 93 k, and (g) 300 k T cells per gel. (h) Release profiles of fluoroparticles from Alg-S-S-PEG or Alg-PEG gels loaded with bone marrow-derived dendritic cells of varied densities. (i) Release profiles of fluoroparticles from Alg-S-S-PEG or Alg-PEG gels loaded with RAW264.7 macrophages (100 k per gel). All the numerical data are presented as mean \pm SD (0.01 < * $P \le 0.05$; ** $P \le 0.01$; *** $P \le 0.01$

k to 100 k and further to 300 k DCs per gel, was not converted to an increased release rate of fluoroparticles from Alg-S-S-PEG and Alg-PEG gels (Fig. 3h). We also tested the release kinetics of microparticles from RAW264.7 macrophage-loaded gels, which again showed a negligible difference between Alg-S-S-PEG gels and Alg-PEG gels (Fig. 3i). RAW264.7 macrophage-loaded Alg-S-S-PEG gels remained intact after 96 h incubation (Fig. 3i). These experiments substantiated T cell-triggered disruption of Alg-S-S-PEG gel network and release of encapsulated microparticles.

2.4. Macroporous Alg-S-S-PEG gels for in vitro expansion of T cells

After confirming that the encapsulated microparticles can be released from Alg-S-S-PEG gels in a T cell-responsive manner, we next studied whether T cells can be stimulated and proliferated in gels encapsulating anti-CD3/CD28-bounded dynabeads. Dynabeads were mixed with Alg-N₃, prior to crosslinking by DBCO-S-S-PEG or DBCO-PEG at $-20~^{\circ}\text{C}$ to form the dynabead-dispersed macroporous gels. CD8 $^{+}$ T cells isolated from C57BL/6 mice were stained with carboxyfluorescein

diacetate succinimidyl ester (CFSE) and loaded into macroporous Alg-S-S-PEG or Alg-PEG gels. Macroporous Alg-S-S-PEG gels with embedded dynabeads successfully proliferated the loaded CFSE-stained CD8⁺ T cells (Fig. 4a). Compared to Alg-PEG gels, Alg-S-S-PEG gels enabled significantly faster expansion of T cells (Fig. 4b and c), presumably due to T cell-mediated release of dynabeads into macropores and subsequent activation of T cells in situ. By increasing the density of loaded T cells from 50 k to 150 k and further to 300 k per gel, a significantly faster T cell proliferation was still observed in Alg-S-S-PEG gels than in Alg-PEG gels (Fig. 4d-g). It is noteworthy that compared to gels loaded with 300 k or 150 k T cells, Alg-S-S-PEG gels loaded with 50 k T cells showed a comparable T cell expansion rate (Fig. 4b-g), demonstrating the ability of Alg-S-S-PEG gels to expand a small amount of T cells in situ. The foldexpansion of CD8+ T cells over time further confirmed the improved stimulation and proliferation of CD8⁺ T cells within the Alg-S-S-PEG gels in comparison with the Alg-PEG gels (Fig. 4h). We also measured the cytokine release profile of OT-1 cells (a type of SIINFEKL-specific CD8+ T cells) expanded by dynabead-loaded Alg-S-S-PEG gels or suspending dynabeads (Fig. 4i and Fig. S7a), which showed negligible differences

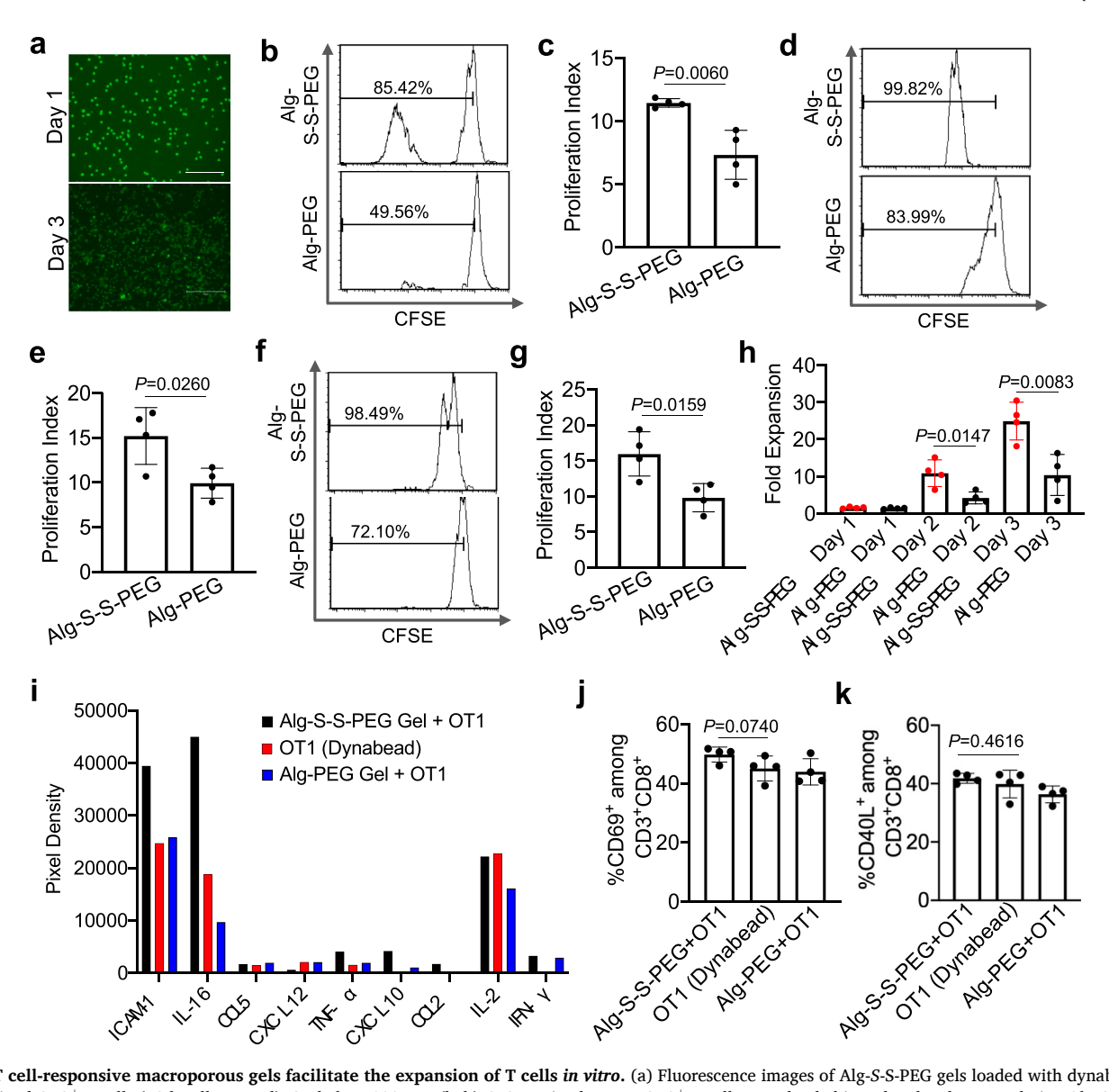


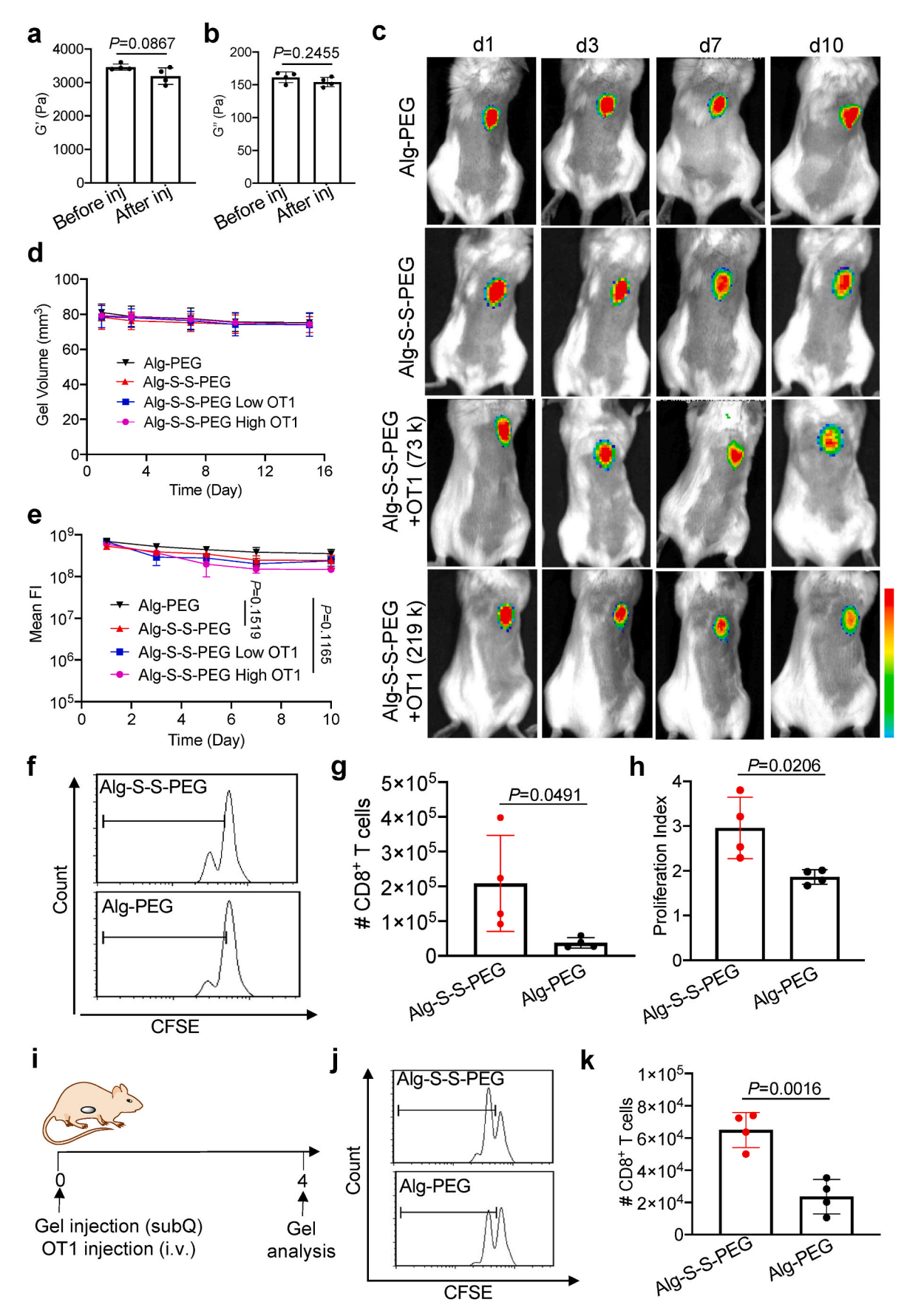
Fig. 4. T cell-responsive macroporous gels facilitate the expansion of T cells *in vitro*. (a) Fluorescence images of Alg-S-S-PEG gels loaded with dynabeads and CFSE-stained CD8⁺ T cells (50 k cells per gel). Scale bar: $100 \, \mu m$. (b–h) CFSE-stained mouse CD8⁺ T cells were loaded into dynabead-encapsulating Alg-S-S-PEG or Alg-PEG gels and incubated at 37 °C for 3 days, prior to flow cytometry analyses. (b) Representative histogram and (c) proliferation index of CD8⁺ T cells in gels loaded with $50 \, k$ T cells initially. (d) Representative histogram and (e) proliferation index of CD8⁺ T cells in gels loaded with $150 \, k$ T cells initially. (f) Representative histogram and (g) proliferation index of CD8⁺ T cells in gels loaded with $300 \, k$ T cells initially. (h) Fold-expansion of CD8⁺ T cells in Alg-S-S-PEG or Alg-PEG gels (50 k cells per gel) over time. (i) Cytokine expression profiles of OT-1 cells expanded by dynabead-loaded Alg-S-S-PEG gels (black), dynabeads (red), or dynabead-loaded Alg-PEG gels (blue). Also shown are percentages of (j) CD69⁺ OT-1 cells and (k) CD40L⁺ OT-1 cells after three-day expansion by dynabead-loaded Alg-S-S-PEG gels, dynabeads, or dynabead-loaded Alg-PEG gels. All the numerical data are presented as mean \pm SD (0.01 < *P \leq 0.00; **P \leq 0.001). (For interpretation of the references to colour in this figure legend, the reader is referred to the Web version of this article.)

for most cytokines examined. We have also measured and compared the surface activation markers (CD69 and CD40L) of OT-1 cells expanded by dynabead-loaded Alg-S-S-PEG gels, dynabeads, or dynabead-loaded Alg-PEG gels, which again showed negligible differences between different groups (Fig. 4j and k). It is noteworthy that OT-1 cells showed similar proliferation rates in the presence of dynabeads or dynabead-loaded Alg-S-S-PEG gels (Fig. S7b-c). These experiments, together with the above T-cell responsive microparticle release experiments, demonstrated that Alg-S-S-PEG gels can release dynabeads in a T cell-responsive manner for subsequent expansion of T cells within the macroporous gel.

2.5. Macroporous Alg-S-S-PEG gels for in situ expansion of T cells

Prior to studying the in vivo expansion of T cells, we investigated the

in vivo stability of fluoroparticle-loaded Alg-S-S-PEG gels. Alg-S-S-PEG gels and Alg-PEG gels could be injected via a 16-gauge needle, with negligible changes in the storage modulus and loss modulus after injection (Fig. 5a and b). We next studied the stability of gels and release kinetics of Sky blue fluoroparticles (3.5 μm in diameter, $\lambda_{\rm ex}/\lambda_{\rm em} = 665/705$ nm) from gels *in vivo*. Balb/c mice were divided into 4 groups and subcutaneously injected with fluoroparticle-loaded Alg-PEG gels, fluoroparticle-loaded Alg-S-S-PEG gels, fluoroparticle/T cell-loaded Alg-S-S-PEG gels (73 k T cells per gel), and fluoroparticle/T cell-loaded Alg-S-S-PEG gels (219 k T cells per gel), respectively. Both gel volume and fluorescence signal were monitored over time. The volume of gels showed negligible changes over time (Fig. 5c and d), demonstrating the good stability of subcutaneously injected Alg-PEG and Alg-S-S-PEG gels *in vivo*. IVIS imaging also showed negligible differences in the fluorescence intensity of gels among different groups (Fig. 5e), indicating the



(caption on next page)

Fig. 5. T cell-responsive macroporous gels facilitate the expansion of T cells *in vivo*. (a) Storage modulus of Alg-S-S-PEG gels before and after injection through a 16-gauge needle. (b) Loss modulus of Alg-S-S-PEG gels before and after injection through a 16-gauge needle. (c) IVIS images of mice at different times post injection of Alg-PEG gels, Alg-S-S-PEG gels, Alg-S-S-PEG gels loaded with 73 k OT-1 cells, or Alg-S-S-PEG gels loaded with 219 k OT-1 cells. Sky blue fluoroparticles (3.5 μm in diameter, $\lambda_{\rm ex}/\lambda_{\rm em} = 665/705$ nm) were encapsulated in each gel. (d) The change of gel volume as in (c) over time post subcutaneous injection. (e) Mean fluorescence intensity of gels as in (c) over time. (f–h) Alg-S-S-PEG or Alg-PEG gels loaded with OT-1 cells (65 k cells per gel) and dynabeads were subcutaneously injected into the flank of mice on day 0, followed by analysis of gels on day 4. (f) Representative histograms of CFSE-stained OT-1 cells harvested from gels. (g) Total number of CD8⁺ T cells in gels at 4 days post gel injection. (i–k) Alg-S-S-PEG or Alg-PEG gels loaded with dynabeads were subcutaneously injected into the flank of mice on day 0, followed by the intravenous injection of CFSE-stained OT-1 cells (65 k cells) on the same day and the analysis of gels on day 4. (i) Timeframe of the study. (j) Representative histograms of CFSE-stained OT-1 cells harvested from gels. (k) Total number of CD8⁺ T cells in gels at 4 days post gel injection. All the numerical data are presented as mean ± SD (0.01 < *P ≤ 0.05; **P ≤ 0.01; ***P ≤ 0.001). (For interpretation of the references to colour in this figure legend, the reader is referred to the Web version of this article.)

good retention of micron-sized fluoroparticles in macroporous Alg-S-S-PEG or Alg-PEG gels. Despite the presence of T cells that can cleave the disulfide linkages, Sky blue fluoroparticles retained well in Alg-S-S-PEG gels (Fig. 5d and e), presumably due to the limited diffusion of micron-sized fluoroparticles out of the gel *in vivo*.

We next studied whether macroporous Alg-S-S-PEG gels loaded with dynabeads enable in situ expansion of T cells. OT-1 cells, a type of SIINFEKL-specific CD8⁺ T cells that can recognize SIINFEKL-expressing cancer cells [38], were used. C57BL/6 mice were subcutaneously injected with Alg-S-S-PEG or Alg-PEG gels containing dynabeads and CFSE-stained OT-1 cells. At 4 days post gel injection, CD8⁺ T cells in Alg-S-S-PEG gels showed a significantly higher expansion rate than in Alg-PEG gels (Fig. 5f), with a higher total number and proliferation index (Fig. 5g and h), demonstrating the ability of dynabead-loaded Alg-S-S-PEG gels to stimulate and expand T cells in situ. To further confirm the in situ T cell expansion property of Alg-S-S-PEG gels in the context of standard T cell therapy, we subcutaneously injected dynabead-loaded Alg-S-S-PEG or Alg-PEG gels into C57BL/6 mice, followed by intravenous injection of CFSE-stained OT-1 cells (Fig. 5i). After 4 days, CD8⁺ T cells in Alg-S-S-PEG again exhibited a higher expansion rate than cells in Alg-PEG gels (Fig. 5j and k), further confirming the ability of macroporous Alg-S-S-PEG gels to expand T cells in situ.

2.6. Macroporous Alg-S-S-PEG gels for improving antitumor efficacy

After demonstrating that macroporous Alg-S-S-PEG gels loaded with dynabeads can expand T cells in situ, we next explored its promise to improve systemic CD8⁺ T cell responses and antitumor efficacy. C57BL/ 6 mice were subcutaneously injected with dynabead- and OT-1-loaded Alg-S-S-PEG or Alg-PEG gels, and SIINFEKL-specific CD8⁺ T cells (i.e., OT-1 cells) in peripheral blood mononuclear cells (PBMCs) were monitored (Fig. 6a). At 3, 6, and 15 days, respectively post injection of OT-1loaded gels, a higher number of SIINFEKL-specific CD8⁺ T cells was detected in mice treated with Alg-S-S-PEG gels than the Alg-PEG gel group or OT-1 cell only group (Fig. 6b-e, Fig. S8), demonstrating the ability of Alg-S-S-PEG gels to expand T cells in situ and increase the systemic level of functional T cells. To further evaluate whether the enhanced in situ expansion of OT-1 cells by Alg-S-S-PEG gels can impart improved tumor control, mice receiving the abovementioned treatment were challenged by subcutaneous injection of E.G7-OVA tumor cells. Compared to the untreated group, all the treatment groups resulted in a slower tumor growth rate (Fig. 6f, Fig. S9). Compared to OT-1-loaded Alg-PEG gels or OT-1 cell alone, mice treated with OT-1-loaded Alg-S-S-PEG gels showed significantly improved survival (Fig. 6g). OT-1loaded Alg-S-S-PEG gels resulted in tumor-free progression in 80% mice, in comparison to 20% in OT-1-loaded Alg-PEG group, 0% in OT-1 cell alone group, and 0% in untreated group (Fig. 6g).

In a therapeutic setting, C57BL/6 mice bearing established E.G7-OVA tumors were subcutaneously injected with OT-1 and dynabead-loaded Alg-S-S-PEG or Alg-PEG gels (250 k per gel) or intravenously injected with a mixture of OT-1 cells (1.25 million) and dynabeads. Alg-PEG treatment failed to slow the tumor growth or prolong animal survival in comparison with the untreated group (Fig. 6h and i). Compared to the untreated group or Alg-PEG gel group, Alg-S-S-PEG gel treatment

significantly reduced the tumor growth rate and prolonged the survival of animals (Fig. 6h and i). Compared to mice treated with the mixture of OT-1 cells and dynabeads with a 5-fold cell dose, Alg-S-S-PEG gel treatment resulted in a comparable antitumor efficacy (6h-i). It is noteworthy that Alg-S-S-PEG gel loaded with dynabeads and OT-1 cells did not cause any noticeable toxicity compared to the untreated group (Fig. S10). We also compared the number and activation status of intratumoral DCs and CD8⁺ T cells in mice subcutaneously administered with OT-1-loaded Alg-S-S-PEG gels or intravenously injected with OT-1 cells (Fig. S11a). Compared to intravenously injected OT-1 cells, OT-1loaded Alg-S-S-PEG gels were able to improve the tumoral infiltration of DCs and CD8⁺ T cells (Fig. S11b, S11d). Intratumoral DCs and CD8⁺ T cells also exhibited an improved activation status in mice treated with OT1-loaded Alg-S-S-PEG gels than mice receiving intravenous injection of OT-1 cells (Fig. S11c, S11e). These experiments well demonstrated that T cell-responsive, macroporous Alg-S-S-PEG gels encapsulating dynabeads can induce the expansion of functional T cells in situ and impart improved antitumor efficacy, in comparison with the nonresponsive gels.

3. Discussion

Material systems that enable in situ expansion of functional T cells hold great promise for shortening the manufacturing process of T cell products and improving the activation of T cells post adoptive transfer [18]. Here we developed a T cell-responsive macroporous hydrogel system for in situ expansion of functional T cells. The macroporous hydrogel contains two types of pores: macropores with an average size of $\sim \! 150 \; \mu m$ and nanosized gel mesh. Microparticles such as dynabeads bearing T cell activation cues (3–5 μm) can be encased by the nanosized gel mesh with minimal background release. The macropores are large enough to home and retain a number of T cells (\sim 10 μ m in diameter). In view of the abundant thiol groups on the surface of T cells, especially activated T cells, we incorporated the disulfide linkages into the gel network of macroporous Alg-S-S-PEG gels. T cells residing in the macropores can gradually cleave the disulfide bonds surrounding the macropores and disrupt the gel network (Fig. 3a-c), resulting in release of encapsulated microparticles into the macropores (Fig. 3e-g). The dynabeads released in response to T cells were able to stimulate and proliferate T cells in the macropores (Fig. 4). DCs and macrophages, in contrast, failed to disrupt the gel network and induce the release of encapsulated microparticles (Fig. 3h and i). It is noteworthy that 15 k T cells per gel (~6 mm in diameter and ~2 mm in height), which corresponds to 266 cells per mm³, were able to disrupt the gel network and induce the release of microparticles from the gel network. At this T cell density, gels remained intact and well preserved the macroporous structure. The ability of the macroporous hydrogels to expand T cells while staying intact holds great promise for in vivo applications.

We show that macroporous Alg-S-S-PEG gels loaded with dynabeads can expand T cells *in vitro* and *in vivo* and improve tumor control. This gel system shows promise to achieve comparable antitumor efficacy to conventional T cell therapy with a much smaller cell dose (Fig. 6h and i). In addition to direct loading of T cells, the T cell-responsive macroporous gels can also be utilized to stimulate systemically injected T cells

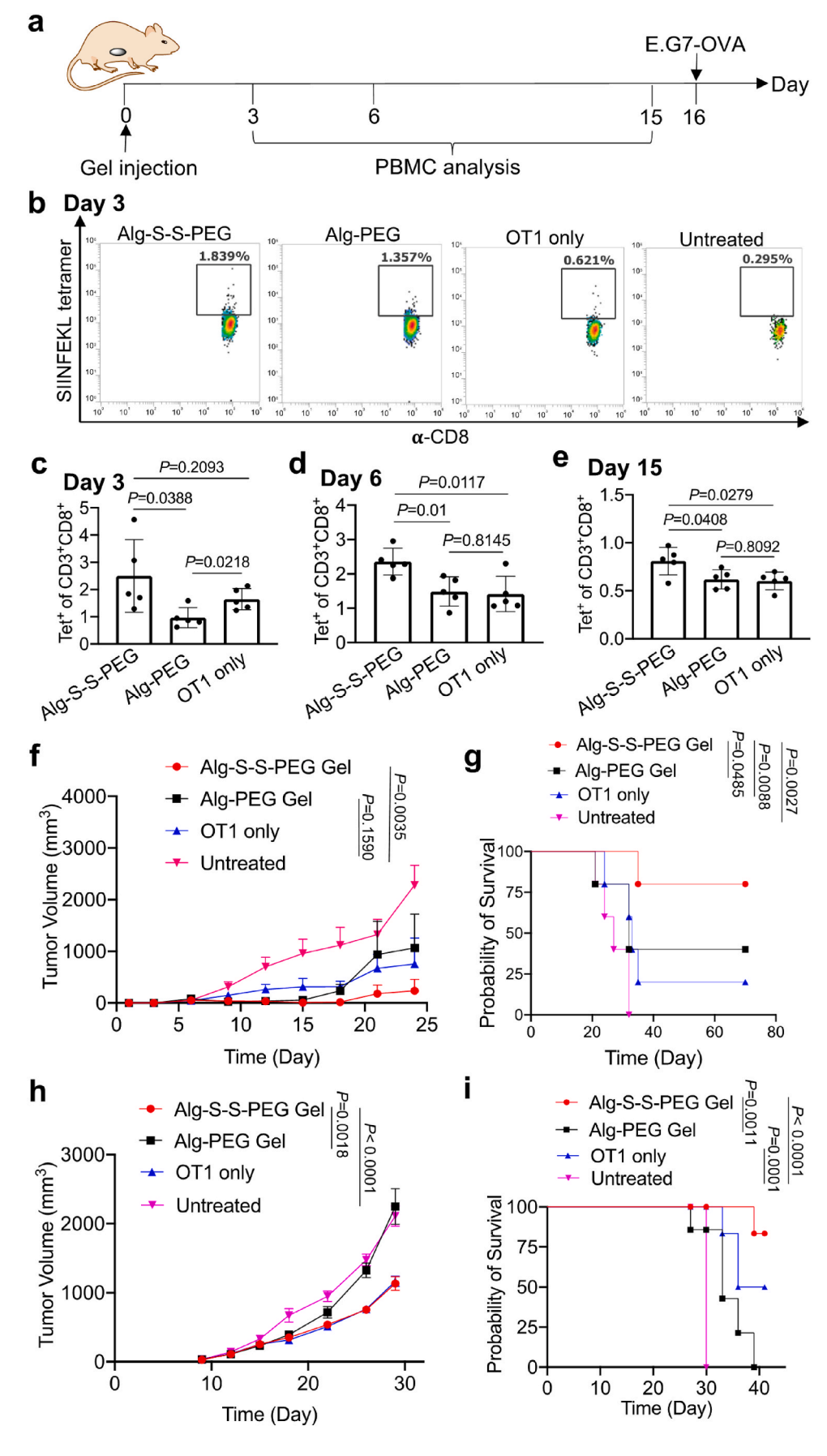


Fig. 6. T cell-responsive macroporous gels can improve the CTL response and antitumor efficacy of functional CD8+ T cells. (a-e) Alg-S-S-PEG or Alg-PEG gels loaded with dynabeads and OT-1 cells were subcutaneously injected into the flank of C57BL/6 mice on day 0, followed by the analysis of SIINFEKL-tetramer⁺ CD8⁺ T cells in PBMCs. Mice injected with OT-1 cells only were used as controls (n = 5). E.G7-OVA tumor cells were inoculated on day 15. (a) Timeframe of the vaccination and prophylactic tumor study. (b) Representative SIINFEKL-tetramer plots of CD8+ T cells in PBMCs at 3 days post gel injection. Also shown are the percentages of SIINFEKL tetramer+ cells among CD8⁺ T cells in PBMCs on (c) day 3, (d) day 6, and (e) day 15, respectively. (f) Average E.G7-OVA tumor volume of each group over the course of prophylactic tumor study. (g) Kaplan-Meier plots for all groups. (h-i) C57BL/6 mice bearing established E.G7-OVA tumors were subcutaneously injected with Alg-S-S-PEG or Alg-PEG gels loaded with dynabeads and OT-1 cells (250 k). Mice intravenously injected with OT-1 cells (1.25 million) and dynabeads were used as controls. (h) Average EG7-OVA tumor volume of each group over the course of the therapeutic tumor study. (i) Kaplan-Meier plots for all groups. All the numerical data are presented as mean \pm SD except for (f) and (h) where mean \pm SEM was used (0.01 $< *P \le 0.05; **P \le 0.01; ***P$ \leq 0.001).

that reach the gel site (Fig. 5i–k). Adoptively transferred T cells can also potentially be actively recruited to the gel site for subsequent *in situ* activation and expansion of T cells, which will be further pursued in future studies [39–42]. This strategy potentially brings minimal obstruction to the manufacturing process of conventional T cell therapies (e.g., CAR T therapy), while providing a facile approach to stimulate and expand engineered T cells *in vivo*. We also envision the feasibility of incorporating CAR-encoded viral particles into the macroporous gels for *in situ* genetic modification and expansion of endogenous T cells [43–45]. These approaches not only hold the promise to develop T cell therapies with improved efficacy, but may also enable us to eventually move the *ex vivo* T cell manufacturing process to *in vivo*.

In this study, we utilize thiols abundant on the surface of T cells to trigger the disruption of Alg-S-S-PEG gel network and subsequent release of encapsulated microparticles into the macropores. The decrease of storage moduli and increase of microparticle release rates in the presence of T cells instead of dendritic cells or macrophages supported the T cell-responsiveness of macroporous Alg-S-S- PEG gels (Fig. 3). However, we are aware that thiols as the trigger are not specific to T cells. The specificity towards T cells can be potentially further improved by taking advantage of enzymes secreted by T cells and utilizing enzyme-degradable linkages to construct the polymeric gel network [46–48]. However, a fine balance between the specificity and efficiency of T cell-responsiveness also needs to be reached, as the use of a highly-specific chemistry might be at the sacrifice of gel degradation kinetics and ease of materials fabrication.

4. Conclusion

To conclude, we developed macroporous Alg-S-S-PEG gels that enable controlled release of T cell activation cues in a T cell-responsive manner and subsequent *in situ* expansion of T cells. Macroporous Alg-S-S-PEG gels can easily load T cells in the macropores and encapsulate microparticles bearing T cell-activation cues (e.g., dynabeads) in the nanosized gel mesh. While exhibiting minimal background release, microparticles can be released into the macropores in the presence of T cells that can gradually disrupt the gel network, for subsequent expansion of T cells *in situ*. We further demonstrated that Alg-S-S-PEG gels loaded with dynabeads can expand functional CD8⁺ T cells *in vivo* for improved tumor control in both prophylactic and therapeutic settings. The ability of T cell-responsive, macroporous Alg-S-S-PEG gels to expand effector T cells in a controlled manner holds promise to reshape the paradigm of current T cell therapies.

5. Methods

Materials and Instrumentation. Sodium alginate, 11-Azido-3,6,9trioxaundecan-1-amine, dicyclohexyl carbodiimide, ysuccinimide, and other chemical reagents were purchased from Sigma Aldrich (St. Louis, MO, USA) unless otherwise noted. 8-Arm PEG-amine was purchased from JenKem Technology USA (Plano, TX, USA). DBCO-S-S-NHS and DBCO-NHS were purchased from Click Chemistry Tools (Scottsdale, AZ, USA). SPHERO Fluorescent Pink or Sky-blue Particles (Fluoroparticles) were purchased from Spherotech, Inc. (Lake Forest, IL, USA). Recombinant murine GM-CSF was purchased from PeproTech, Inc. (Cranbury, NJ, USA). Primary antibodies used in this study, including anti-CD11b, anti-CD11c, anti-CD3, anti-CD8 and Fixable viability dye efluor780, were obtained from Thermo Fisher Scientific (Waltham, MA, USA). All antibodies were diluted according to the manufacturer's recommendations. Mouse CD3+ T cell isolation kit, dynabeads, and LS separation columns were purchased from Miltenyi Biotec (Bergisch Gladbach, Germany). Proteome Profiler Mouse Cytokine Array Kit, Panel A (R&D, USA). FACS analyses were collected on Attune NxT or BD LSR Fortessa flow cytometers and analyzed on FlowJo v7.6 and FCS Express v6 and v7. Statistical testing was performed using GraphPad Prism v6 and v8. Fluorescence measurement was conducted

on a plate reader. Small compounds were run on the Shimadzu LC40 ultra high performance liquid chromatography/mass spectrometer. Proton nuclear magnetic resonance spectra were collected on the Varian U500 or VXR500 (500 MHz) spectrometer. Scanning electron microscopic images were taken with a Hitachi S-4800 High Resolution Scanning Electron Microscope. Mechanical tests were performed on an AR-G2 rheometer (TA Instruments, New Castle, DE, USA).

Cell lines and animals. The EG7-OVA cell line was purchased from American Type Culture Collection (Manassas, VA, USA). Cells were cultured in DMEM containing 10% FBS, 100 units/mL Penicillin G, 100 $\mu g/mL$ streptomycin, and 50 $\mu g/mL$ G418 at 37 °C in 5% CO_2 humidified air. Female C57BL/6 and OT-1 mice were purchased from the Jackson Laboratory (Bar Harbor, ME, USA). Feed and water were available ad libitum. Artificial light was provided in a 12 h/12 h cycle. All procedures involving animals were done in compliance with National Institutes of Health and Institutional guidelines with approval from the Institutional Animal Care and Use Committee at the University of Illinois at Urbana-Champaign.

Synthesis of Alg-N₃. Sodium alginate was dissolved in deionized water overnight. 1-Ethyl-3-(3-dimethylaminopropyl)carbodiimide and N-hydroxysuccinimide were added and stirred for 1 h at room temperature. 11-Azido-3,6,9-trioxaundecan-1-amine was then added, and the reaction mixture was stirred for another 24 h. The reaction solution was filtrated and dialyzed against NaCl solution and deionized water. The dialysis medium was changed every 12 h for 4 times. Finally, the purified polymer solution was filtered, lyophilized, and stored at $-20\,^{\circ}\mathrm{C}$ until use

Synthesis of DBCO-S-S-PEG or DBCO-PEG. DBCO-S-S-NHS or DBCO-NHS (8 $\mu mol)$ was dissolved in 300 μL of methanol. A solution of 8-Arm-PEG-NH2 (MW 40 k) (1 $\mu mol)$ in 5 mL of water was added, and the mixture was stirred for 30 min NaHCO3 (8 μmol) was then added and the mixture was stirred for another 24 h, followed by the ultracentrifugation (3000 Da Amicon filter) of the mixture to remove small molecules. Further purification was performed by washing with deionized water for at- least three times.

Fabrication of macroporous Alg-S-S-PEG or Alg-PEG gels. Alg-N $_3$ (20 mg/mL) and DBCO-S-S-PEG (or DBCO-PEG, 27 mg/mL) were separately dissolved in deionized water and loaded into two syringes. Alg-N $_3$ and DBCO-S-S-PEG were then quickly mixed for $\sim\!30$ s with a 10:1 vol ratio using a Luer lock connector. After mixing, the solution was injected into a cylindrical shape mold and kept at $-20~^\circ\mathrm{C}$ for overnight. After 6 h or longer when the polymerization was complete, gels were brought back to room temperature for the ice crystals to melt, resulting in the formation of macroporous hydrogels.

Pore size measurement. Macroporous hydrogels were immersed in PBS and placed under the optical microscope. At least 50 images were taken for different regions of the macroporous hydrogel. For each image, the pore size was measured with the assistance of ImageJ and averaged. These averaged numbers were then further averaged over at least 50 images to calculate the pore size of macroporous hydrogels.

Porosity measurement. Macroporous gels were placed in 1 mL of deionized water at ambient condition for a few hours. Gel wicking assay was performed using an absorbent Kimwipe (Kimberly-Clark) to touch only one side of the gel, allowing the water inside the pores to be drawn out by capillary force. The initial gel weight (W_i) and the final gel weight after the wicking assay (W_f) were measured. Porosity was calculated as the percentage of (W_i - W_f)/ W_i .

SEM imaging of macroporous hydrogels. Hitachi S-4800 high-resolution Scanning Electron Microscope (SEM) was used to image the macroporous hydrogel. To prepare SEM samples, hydrogels were fixed with 4% paraformaldehyde (PFA) in PBS for 20 min, transferred to PBS for 5 min to wash off PFA, then transferred to water for 5 min, water for 10 min, 30% ethanol for 5 min, 30% ethanol for 5 min, 50% ethanol for 10 min, 70% ethanol for 5 min, 70% ethanol for 10 min, 90% ethanol for 5 min, 100% ethanol for 5 min, 100% ethanol for 5 min, 11:1 ethanol HMDS for 5 min, HMDS

for 2 min, and HMDS for 2 min. The samples were crudely dried with Kimwipe and then placed in a desiccator for overnight.

Mechanical tests of gels. The storage and loss moduli of macroporous hydrogels were extracted from strain sweep tests at 1 Hz followed by a frequency sweep test at 0.5% strain under ambient condition on an AR-G2 rheometer (TA Instruments). An 8 mm flat plate geometry equipped with a bottom Peltier plate on the instrument was used to test all the samples with the same procedure file. A loading gap of approximately 1600 μm was used for each test. Any kind of spill over while running the test was avoided by trimming the edges as needed. No pretreatment or stress was applied to any sample for any measurement.

Release of fluoroparticles from gels in response to DTT. Fluoroparticle-loaded macroporous gels were fabricated by codissolving SPHERO and Alg-N $_3$ polymer for 12 h, and crosslinking them with DBCO-S-S-PEG or DBCO-PEG at $-20\,^{\circ}$ C. The gels were placed in a 48-well flat bottom plate and immersed in 500 μ L of PBS containing dithiothreitol (DTT) at room temperature under continuous shaking. At selected time points, 100 μ L aliquots of supernatants were sampled for fluoroparticle quantification on a plate reader.

Isolation of CD8 $^+$ T cells and OT-1 cells. CD8 $^+$ T and OT-1 cells were sorted from spleens of mice under aseptic condition. Spleen was placed on a 40 μ m cell strainer, grinded with the sponge end of a syringe, and flushed with 10 mL of RPMI medium. Cells were collected and centrifuged, followed by the removal of supernatants. Cell pellets were then resuspended in 1 mL of red blood cell (RBC) lysis buffer, incubated at room temperature for 2 min, and diluted with 10 mL of PBS. Cells were centrifuged, re-suspended in PBS, and counted, prior to T cell isolation. CD8 $^+$ T cells or OT-1 cells were isolated via negative selection (CD8a $^+$ T Cell Isolation Kit, Miltenyi Biotec) following the manufacturer's instructions.

Preparation of bone marrow-derived dendritic cells. Tibia and femur of C57 BL/6 mice were collected from mice and placed in RPMI medium containing high concentration of Penicillin G/Streptomycin. After the removal of muscles and connective tissues, the top and bottom of tibia and femur were cut open. The whole bone marrow was flushed out using 10 mL of RPMI media in a 10 mL syringe with a 23G needle. The clumps of bone marrow were dissociated by drawing into a syringe with an 18G needle and pushing it back to the Petri dish for a few times until no clumps were visible. Bone marrow cells were then filtered through a 70 µm cell strainer. After cell counting and centrifugation, cells were resuspended at 2×10^6 cells/mL in RPMI 1640 containing 2 mM L-glutamine, Sodium bicarbonate, 10% Heat-inactivated FBS, 2mercaptoethanol, 1% penicillin/streptomycin, and GM-CSF, and placed in an incubator (37 °C, 5% CO₂). 10 mL of fresh medium was added on day 3 and day 6. Bone marrow-derived dendritic cells were ready for use from day 7.

CFSE staining of T cells. PBS was warmed before use. The stock solution (10 mM) of CFSE (Invitrogen) was diluted in warm PBS to 1 μM (1 μL of stock in 10 mL of PBS). T cells were quickly added to CFSE solution with a cell density of $10^6/mL$ and incubated for 15 min at 37 °C. Pellets of cells were collected by centrifugation, resuspended in fresh prewarmed T-cell medium, and further incubated for another 30 min at 37 °C to ensure thorough staining. Cells were then washed with PBS and resuspended for use.

Release of fluoroparticles from gels in response to T cells. Fluoroparticle-loaded gels were placed in a 96-well flat bottom plate. Absorbent Kimwipe was used to touch the side of the gel, allowing the water inside the pores to be drawn out by capillary force. $\sim\!20{-}25~\mu L$ of T cells (50 k, 93 k, or 300 k) in medium was added to the surface of gel, allowing gels to absorb the medium containing T cells. The gels were then immersed in 500 μL of T cell medium and incubated at 37 °C. At selected time points, 100 μL aliquots of supernatants were sampled for fluoroparticle quantification on a plate reader. The same procedure and measurements were performed DCs and RAW 264.7 cells.

Mechanical tests of T cell-loaded gels. Macroporous Alg-S-S-PEG or Alg-PEG gels were loaded with T cells of different densities or blank

medium, and incubated at 37 $^{\circ}\text{C}$ for 24 h. Gels were then harvested for mechanical tests on an AR-G2 rheometer (TA Instruments), following the abovementioned protocol.

Mechanical tests of DTT-treated gels. Macroporous Alg-S-S-PEG or Alg-PEG gels were incubated with DTT of varying concentrations (10, 100, or 500 μ M) at room temperature for 72 h. After 72 h, gels were harvested for mechanical tests on an AR-G2 rheometer (TA Instruments), following the abovementioned protocol.

Mechanical tests of gels before and after injection. Macroporous Alg-S-S-PEG or Alg-PEG gels were injected via a 16-gauge needle into a circular plate. Gels before and after injection were harvested for mechanical tests on an AR-G2 rheometer (TA Instruments), following the abovementioned protocol.

In vivo release of fluoroparticles from gels in response to T cells. Sky blue fluoroparticle-loaded Alg-S-S-PEG and Alg-PEG gels were prepared following the abovementioned procedure. Absorbent Kimwipe was used to touch the side of the gel, allowing the water inside the pores to be drawn out by capillary force. $\sim\!20{\text -}25~\mu\text{L}$ of OT-1 cells (73 k or 219 k) in the medium was added to the surface of the gel, allowing gels to absorb the medium containing OT-1 cells. The gels (with or without OT-1 cells) were then subcutaneously injected into the flank of Balb/6 mice via a 16G needle. At selected time points, images of mice were taken on an IVIS Imaging System to monitor the retention of fluoroparticles.

In vitro T cell proliferation Assay. Dynabead-loaded macroporous gels were prepared by co-dissolving dynabeads and Alg-N $_3$, and cross-linking them with DBCO-S-S-PEG or DBCO-PEG at $-20\,^{\circ}\text{C}$. The gels were placed in a 96-well flat bottom plate. Absorbent Kimwipe was used to touch the side of the gel, allowing the water inside the pores to be drawn out by capillary force. CSFE-stained T cells of different cell densities were then added to the surface of gels, allowing gels to absorb the medium containing T cells. 200 μL of T cell medium was added, and the plate was incubated at 37 $^{\circ}\text{C}$ for 3 days before flow cytometry and fluorescence imaging analyses.

In vivo T cell Proliferation Assay. Dynabead-loaded macroporous gels were prepared by co-dissolving dynabeads and Alg-N₃, and cross-linking them with DBCO-S-S-PEG or DBCO-PEG at $-20\,^{\circ}\text{C}$. Gels were taken out at room temperature and absorbent Kimwipe was used to touch the side of the gel, allowing the water inside the pores to be drawn out by capillary force. CSFE-stained T cells (~65 k) were then added to the surface of gels, allowing gels to absorb the medium containing T cells. Gels loaded with T cells were then subcutaneously injected into the flank of C57BL/6 mice via a 16G needle. For some groups, T cells were i. v injected. The proliferation of T cells was evaluated by harvesting the gel from mice for FACS assay after 4 days.

Harvesting gels from mice for FACS analysis. Gels were isolated from mice, placed on a 40 μm cell strainer, grinded with the sponge end of a syringe, and flushed with 10 mL of RPMI medium. Cells were collected and centrifuged, followed by the removal of supernatants. Cell pellets were then re-suspended in PBS, washed, and counted. Further, cells were added to 96-well plates for antibody staining and FACS analysis.

Cytokine analysis. The cytokine release profile of T cells was analyzed using a proteome profiler assay (Proteome Profiler Mouse Cytokine Array Kit, Panel A). Briefly, OT1 cells (100 k) were incubated within dynabead-loaded Alg-S-S-PEG gels or Alg-PEG gels or with suspending dynabeads for 3 days. The culture medium was collected, centrifuged to remove dead cells and cell debris, and used for cytokine analysis. All the reagents were prepared following the manufacturer's protocol (R&D, USA). Briefly, the membranes were incubated with Array Buffer 6 (for blocking) for 1 h on a shaker. Samples were prepared by adding up to 1 mL of each sample to 0.5 mL of Array Buffer 4 in separate tubes. The final volume was adjusted to 1.5 mL with Array Buffer 6 as necessary. Then, 15 μ L of mouse cytokine detection antibody cocktails were added to each prepared sample and incubated for 1 h. Then, the membrane was washed with Array Buffer 6 and incubated with the antibody mixture sample at 4 °C overnight. The next day, the

membranes were washed followed by incubation with Streptavidin-HRP (1:2000) for 30 min at room temperature. Finally, the membrane was washed again and 1 mL of Chemi Reagent mix was added on top of each membrane. The membrane was exposed to a Chemiluminescence imager for 2–5 min. Therefore, the positive signals obtained in the membranes were identified by placing the transparency overlay template provided by the supplier, on the obtained array image and aligning it with the given reference spots for each cytokine. The Pixel densities (average signals of pair of duplicates) were analyzed using ImageJ and the average background was subtracted respectively.

Tumor analysis after treatment. C57BL/6 mice were divided into three groups: Alg-S-S-PEG Gel with OT-1 cells, OT-1 i. v injection, and no treatment (n = 4). E.G7-OVA cells (250 k) washed in HBSS buffer solution were subcutaneously injected into the upper right flank of the C57BL/6 mice on Day 0. On Day 16, gels loaded with OT-1 cells (250 k) were subcutaneously injected. OT-1 cells (250 k per mouse) injected intravenously were used as the control. On Day 21, tumors were harvested for further analysis. Briefly, tumors were disrupted using a syringe plunger, strained through a 40 μ m cell strainer, and flushed with 10 mL of RPMI. Cells were then collected, washed with PBS, and stained for flow cytometry analysis.

Prophylactic tumor study. OT-1-loaded gels (1.25×10^5) OT-1 cells per gel) were prepared using the abovementioned procedure and subcutaneously injected into the flank of C57BL/6 mice via a 16 G needle. The expansion of OT-1 cells was evaluated by analyzing the levels of SIINFEKL-specific CD8⁺ T cells, i.e., OT-1 cells, at different time points post gel injection. Blood was collected via retro-orbital bleeding. Peripheral blood mononuclear cells were harvested and stained with MHC-I SIINFEKL tetramer, anti-CD3, anti-CD4, anti-CD8, and live/dead stain for 20 min, prior to flow cytometry analyses. To study whether the expanded OT-1 cells can improve the control of tumors, mice were divided into four groups: Alg-S-S-PEG gel loaded with OT-1 cells, Alg-PEG gel loaded with OT-1 cells, OT-1 cells alone, or no treatment. Gels loaded with OT-1 cells were injected on day 0. E.G7-OVA tumor cells (2 \times 10⁵ in 50 μ L HBSS) were subcutaneously (distant from the gel site) injected into mice on day 15. Tumor size was measured every 2-3days, and tumor volume was calculated by $(L \times W [2])/2$ where L is the longest diameter and W is the shortest diameter of tumors.

Therapeutic tumor study. E.G7-OVA tumors were established in C57BL/6 mice by subcutaneous injection of E.G7-OVA cells (0.35 million cells in 50 μL of HBSS) into the right flank. When the tumors reached a diameter of 6–7 mm, mice were randomly divided into four groups: Alg-S-S-PEG gel, Alg-PEG gel, OT-1+dynabeads, and untreated (n = 6 per group). Gels loaded with OT-1 cells (250 k OT-1 cells) and dynabeads were subcutaneously injected into the right flank of the mice. For the third group, 1.25 million OT-1 cells and dynabeads were intravenously injected. Tumor size was measured every 2–3 days, and tumor volume was calculated by (L \times W^[2])/2 where L is the longest diameter and W is the shortest diameter of tumors.

Statistical analyses. Statistical analysis was performed using GraphPad Prism v6 and v8. Sample variance was tested using the F test. For samples with equal variance, the significance between the groups was analyzed by a two-tailed student's *t*-test. For samples with unequal variance, a two-tailed Welch's *t*-test was performed. For multiple comparisons, a one-way analysis of variance (ANOVA) with post hoc Fisher's LSD test was used. The results were deemed significant at $0.01 < *P \le 0.05$, highly significant at $0.001 < *P \le 0.01$, and extremely significant at *** $P \le 0.001$.

CRediT authorship contribution statement

Rimsha Bhatta: Experiments, Methodology, Formal analysis, Writing – original draft. Joonsu Han: Experiments, Methodology. Yusheng Liu: Experiments, Methodology. Yang Bo: Experiments, Methodology. Hua Wang: Supervision, Conceptualization, Formal analysis, Writing – review & editing.

Declaration of competing interest

The authors declare that they have no known competing financial interests or personal relationships that could have appeared to influence the work reported in this paper.

Data availability

Data will be made available on request.

Acknowledgements

The authors would like to acknowledge the financial support from NSF DMR 2143673 CAR, R01CA274738, and the start-up package from the Department of Materials Science and Engineering at the University of Illinois at Urbana-Champaign and the Cancer Center at Illinois. Research reported in this publication was supported by the Cancer Scholars for Translational and Applied Research (C*STAR) Program sponsored by the Cancer Center at Illinois and the Carle Cancer Center under Award Number CST EP012023. Rimsha Bhatta acknowledges the support from the National Institute of Biomedical Imaging and Bioengineering of the National Institutes of Health under Award Number T32EB019944.

Appendix A. Supplementary data

Supplementary data to this article can be found online at $\frac{https:}{doi.}$ org/10.1016/j.biomaterials.2022.121972.

References

- J. Couzin-Frankel, Breakthrough of the year 2013. Cancer immunotherapy, Science 342 (2013) 1432–1433.
- [2] I. Mellman, G. Coukos, G. Dranoff, Cancer immunotherapy comes of age, Nature 480 (2011) 480–489.
- [3] R.C. Sterner, R.M. Sterner, CAR-T cell therapy: current limitations and potential strategies, Blood Cancer J. 11 (2021) 69.
- [4] M. Sadelain, R. Brentjens, I. Rivière, The basic principles of chimeric antigen receptor design, Cancer Discov. 3 (2013) 388–398.
- [5] M. Abou-el-Enein, et al., Scalable manufacturing of CAR T cells for cancer immunotherapy, Blood Cancer Discov 2 (2021) 408.
- [6] X. Wang, et al., Large-scale clinical-grade retroviral vector production in a fixed-bed bioreactor, J. Immunother. 38 (2015) 127–135.
- [7] J.C. van der Loo, et al., Scale-up and manufacturing of clinical-grade self-inactivating γ-retroviral vectors by transient transfection, Gene Ther. 19 (2012) 246–254.
- [8] M. Abou-El-Enein, et al., Good Manufacturing Practices (GMP) manufacturing of advanced therapy medicinal products: a novel tailored model for optimizing performance and estimating costs, Cytotherapy 15 (2013) 362–383.
- [9] M. Abou-El-Enein, G. Bauer, N. Medcalf, H.D. Volk, P. Reinke, Putting a price tag on novel autologous cellular therapies, Cytotherapy 18 (2016) 1056–1061.
- [10] S. Stock, M. Schmitt, L. Sellner, Optimizing manufacturing protocols of chimeric antigen receptor T cells for improved anticancer immunotherapy, Int. J. Mol. Sci. 20 (2019) 6223.
- [11] M. Schluck, R. Hammink, C.G. Figdor, M. Verdoes, J. Weiden, Biomaterial-Based activation and expansion of tumor-specific T cells, Front. Immunol. 10 (2019) 931.
- [12] C. Wang, W. Sun, Y. Ye, H.N. Bomba, Z. Gu, Bioengineering of artificial antigen presenting cells and lymphoid organs, Theranostics 7 (2017) 3504–3516.
- [13] X. Wang, I. Rivière, Clinical manufacturing of CAR T cells: foundation of a promising therapy, Mol. Ther. Oncolytics 3 (2016), 16015.
- [14] A.S. Cheung, D.K.Y. Zhang, S.T. Koshy, D.J. Mooney, Scaffolds that mimic antigenpresenting cells enable ex vivo expansion of primary T cells, Nat. Biotechnol. 36 (2018) 160–169.
- [15] D.K.Y. Zhang, A.S. Cheung, D.J. Mooney, Activation and expansion of human T cells using artificial antigen-presenting cell scaffolds, Nat. Protoc. 15 (2020) 773, 708
- [16] B.L. Levine, J. Miskin, K. Wonnacott, C. Keir, Global manufacturing of CAR T cell therapy, Mol. Ther. Methods Clin. Dev. 4 (2017) 92–101.
- [17] E.J. Wherry, T cell exhaustion, Nat. Immunol. 12 (2011) 492–499.
- [18] A. Isser, N.K. Livingston, J.P. Schneck, Biomaterials to enhance antigen-specific T cell expansion for cancer immunotherapy, Biomaterials 268 (2021), 120584.
- [19] C.T. Tsao, et al., Thermoreversible poly(ethylene glycol)-g-chitosan hydrogel as a therapeutic T lymphocyte depot for localized glioblastoma immunotherapy, Biomacromolecules 15 (2014) 2656–2662.
- [20] A. Monette, C. Ceccaldi, E. Assaad, S. Lerouge, R. Lapointe, Chitosan thermogels for local expansion and delivery of tumor-specific T lymphocytes towards enhanced cancer immunotherapies, Biomaterials 75 (2016) 237–249.

- [21] S.B. Stephan, et al., Biopolymer implants enhance the efficacy of adoptive T-cell therapy, Nat. Biotechnol. 33 (2015) 97–101.
- [22] A.F. Atik, et al., Hyaluronic acid based low viscosity hydrogel as a novel carrier for Convection Enhanced Delivery of CAR T cells, J. Clin. Neurosci. 56 (2018) 163–168.
- [23] E. Hong, et al., Configuration-dependent presentation of multivalent IL-15:IL-15 π 0 enhances the antigen-specific T cell response and anti-tumor immunity, J. Biol. Chem. 291 (2016) 8931–8950.
- [24] J. Park, et al., Combination delivery of TGF-β inhibitor and IL-2 by nanoscale liposomal polymeric gels enhances tumour immunotherapy, Nat. Mater. 11 (2012) 895–905.
- [25] D. Schmid, et al., T cell-targeting nanoparticles focus delivery of immunotherapy to improve antitumor immunity, Nat. Commun. 8 (2017) 1747.
- [26] W. Ou, et al., Regulatory T cell-targeted hybrid nanoparticles combined with immuno-checkpoint blockage for cancer immunotherapy, J. Contr. Release 281 (2018) 84–96.
- [27] O.A. Ali, N. Huebsch, L. Cao, G. Dranoff, D.J. Mooney, Infection-mimicking materials to program dendritic cells in situ, Nat. Mater. 8 (2009) 151–158.
- [28] H. Wang, D.J. Mooney, Biomaterial-assisted targeted modulation of immune cells in cancer treatment, Nat. Mater. 17 (2018) 761–772.
- [29] P.V. Chang, et al., Copper-free click chemistry in living animals, Proc. Natl. Acad. Sci. USA 107 (2010) 1821–1826.
- [30] H. Wang, et al., Selective in vivo metabolic cell-labeling-mediated cancer targeting, Nat. Chem. Biol. 13 (2017) 415.
- [31] V.I. Lozinsky, et al., Polymeric cryogels as promising materials of biotechnological interest, Trends Biotechnol. 21 (2003) 445–451.
- [32] A.J. Thornton, E. Alsberg, E.E. Hill, D.J. Mooney, Shape retaining injectable hydrogels for minimally invasive bulking, J. Urol. 172 (2004) 763–768.
- [33] S.A. Bencherif, et al., Injectable cryogel-based whole-cell cancer vaccines, Nat. Commun. 6 (2015) 7556.

- [34] A. Meister, M.E. Anderson, Glutathione. Annu. Rev. Biochem. 52 (1983) 711-760.
- [35] P. Kesarwani, et al., Promoting thiol expression increases the durability of antitumor T-cell functions, Cancer Res. 74 (2014) 6036–6047.
- [36] L.J. Matthias, et al., Disulfide exchange in domain 2 of CD4 is required for entry of HIV-1, Nat. Immunol. 3 (2002) 727–732.
- [37] L. Tang, et al., Enhancing T cell therapy through TCR-signaling-responsive nanoparticle drug delivery, Nat. Biotechnol. 36 (2018) 707–716.
- [38] H. Wang, et al., Metabolic labeling and targeted modulation of dendritic cells, Nat. Mater. 19 (2020) 1244–1252.
- [39] J.R. Groom, A.D. Luster, CXCR3 in T cell function, Exp. Cell Res. 317 (2011) 620–631.
- [40] N. Karin, CXCR3 ligands in cancer and autoimmunity, chemoattraction of effector T cells, and beyond, Front. Immunol. (2020) 11.
- [41] R. Tokunaga, et al., CXCL9, CXCL10, CXCL11/CXCR3 axis for immune activation—a target for novel cancer therapy, Cancer Treat Rev. 63 (2018) 40–47.
- [42] R.S. Klein, et al., Neuronal CXCL10 directs CD8+ T-cell recruitment and control of West Nile virus encephalitis, J. Virol. 79 (2005) 11457–11466.
- [43] H. Gao, et al., Development of T cells redirected to glypican-3 for the treatment of hepatocellular carcinoma, Clin. Cancer Res. 20 (2014) 6418–6428.
- [44] N.N. Parayath, M.T. Stephan, In situ programming of CAR T cells, Annu. Rev. Biomed. Eng. 23 (2021) 385–405.
- [45] J.T. Huckaby, et al., Bispecific binder redirected lentiviral vector enables in vivo engineering of CAR-T cells, J. Immunother. Cancer 9 (2021), e002737.
- [46] Q. Hu, P.S. Katti, Z. Gu, Enzyme-responsive nanomaterials for controlled drug delivery, Nanoscale 6 (2014) 12273–12286.
- [47] R.V. Ulijn, Enzyme-responsive materials: a new class of smart biomaterials, J. Mater. Chem. 16 (2006) 2217–2225.
- [48] J. Hu, G. Zhang, S. Liu, Enzyme-responsive polymeric assemblies, nanoparticles and hydrogels, Chem. Soc. Rev. 41 (2012) 5933–5949.